Guided-mode resonance gratings for enhanced mid-infrared absorption in quantum dot intermediate-band solar cells

Research Article | Vol. 26, No. 6 | 19 Mar 2018 | OPTICS EXPRESS A352
Optics EXPRESS

Guided-mode resonance gratings for enhanced mid-infrared absorption in quantum dot intermediate-band solar cells

FARID ELSEHRAWY,[1] TAPIO NIEMI,[2] AND FEDERICA CAPPELLUTI[1,*]

[1]*Department of Electronics and Telecommunications, Politecnico di Torino, Torino, 10129, Italy*
[2]*Laboratory of Photonics, Tampere University of Technology, P.O. Box 692, FI-33101 Tampere, Finland*
[*]*federica.cappelluti@polito.it*

Abstract: Achieving strong absorption of low-energy photons is one of the key issues to demonstrate quantum dot solar cells working in the intermediate band regime at practical concentration factors and operating temperatures. Guided-mode resonance effects may enable large enhancement of quantum dot intraband optical transitions. We propose quantum dot thin-film cells designed to have significant field waveguiding in the quantum dot stack region and patterned at the rear-side with a sub-wavelength diffraction grating. Remarkable increase of the optical path length at mid-infrared wavelengths is shown owing to guided-mode resonances. Design guidelines are presented for energy and strength of the second-photon absorption for III-V quantum dots, such as InAs/GaAs and GaSb/GaAs, whose intraband and intersubband transitions roughly extends over the $2-8\ \mu$m range. The proposed design can also be applied to quantum dot infrared detectors. Angle-selectivity is discussed in view of applications in concentrator photovoltaic systems and infrared imaging systems.

OCIS codes: (040.5350) Photovoltaic; (040.3060) Infrared; (040.5160) Photodetectors; (050.1950) Diffraction gratings; (050.6624) Subwavelength structures.

References and links

1. A. Luque and A. Martí, "Increasing the efficiency of ideal solar cells by photon induced transitions at intermediate levels," Phys. Rev. Lett. **78**, 5014–5017 (1997).
2. A. Luque and A. Marti, "The intermediate band solar cell: progress toward the realization of an attractive concept," Adv. Mater. **22**, 160–174 (2010).
3. Y. Okada, N. Ekins-Daukes, T. Kita, R. Tamaki, M. Yoshida, A. Pusch, O. Hess, C. Phillips, D. Farrell, K. Yoshida *et al.*, "Intermediate band solar cells: Recent progress and future directions," Appl. Phys. Rev. **2**, 021302 (2015).
4. A. Mellor, A. Luque, I. Tobías, and A. Martí, "The feasibility of high-efficiency inas/gaas quantum dot intermediate band solar cells," Sol. Energy Mater Sol. Cells **130**, 225–233 (2014).
5. S. Turner, S. Mokkapati, G. Jolley, L. Fu, H. H. Tan, and C. Jagadish, "Periodic dielectric structures for light-trapping in ingaas/gaas quantum well solar cells," Opt. Express **21**, A324–A335 (2013).
6. A. Musu, F. Cappelluti, T. Aho, V. Polojärvi, T. K. Niemi, and M. Guina, "Nanostructures for light management in thin-film gaas quantum dot solar cells," in "Solid-State Lighting," (Optical Society of America, 2016), pp. JW4A45.
7. B. L. Smith, M. A. Slocum, Z. S. Bittner, Y. Dai, G. T. Nelson, S. D. Hellstroem, R. Tatavarti, and S. M. Hubbard, "Inverted growth evaluation for epitaxial lift off (elo) quantum dot solar cell and enhanced absorption by back surface texturing," in "Photovoltaic Specialists Conference (PVSC), 2016 IEEE 43rd," (IEEE, 2016), pp. 1276–1281.
8. H. Feng Lu, S. Mokkapati, L. Fu, G. Jolley, H. Hoe Tan, and C. Jagadish, "Plasmonic quantum dot solar cells for enhanced infrared response," Appl. Phys. Lett. **100**, 103505 (2012).
9. F. Cappelluti, D. Kim, M. van Eerden, A. Cédola, T. Aho, G. Bissels, F. Elsehrawy, J. Wu, H. Liu, and P. Mulder, "Light-trapping enhanced thin-film iii-v quantum dot solar cells fabricated by epitaxial lift-off," Sol. Energy Mater Sol. Cells (in press) (2018).
10. A. Mellor, I. Tobías, A. Martí, and A. Luque, "A numerical study of bi-periodic binary diffraction gratings for solar cell applications," Sol. Energy Mater Sol. Cells **95**, 3527–3535 (2011).
11. S. Wang, M. Moharam, R. Magnusson, and J. Bagby, "Guided-mode resonances in planar dielectric-layer diffraction gratings," JOSA A **7**, 1470–1474 (1990).
12. Y.-C. Lee, C.-F. Huang, J.-Y. Chang, and M.-L. Wu, "Enhanced light trapping based on guided mode resonance effect for thin-film silicon solar cells with two filling-factor gratings," Opt. Express **16**, 7969–7975 (2008).
13. T. Khaleque and R. Magnusson, "Light management through guided-mode resonances in thin-film silicon solar cells," J Nanophotonics **8**, 083995 (2014).

#319866 https://doi.org/10.1364/OE.26.00A352
Journal © 2018 Received 16 Jan 2018; accepted 6 Mar 2018; published 14 Mar 2018

14. C.-C. Wang and S.-D. Lin, "Resonant cavity-enhanced quantum-dot infrared photodetectors with sub-wavelength grating mirror," J. Appl. Phys. **113**, 213108 (2013).
15. J. Tommila, V. Polojärvi, A. Aho, A. Tukiainen, J. Viheriälä, J. Salmi, A. Schramm, J. Kontio, A. Turtiainen, T. Niemi *et al.*, "Nanostructured broadband antireflection coatings on alinp fabricated by nanoimprint lithography," Sol. Energy Mater Sol. Cells **94**, 1845–1848 (2010).
16. E. E. Perl, W. E. McMahon, J. E. Bowers, and D. J. Friedman, "Design of antireflective nanostructures and optical coatings for next-generation multijunction photovoltaic devices," Opt. Express **22**, A1243–A1256 (2014).
17. Y. Harada, T. Maeda, and T. Kita, "Intraband carrier dynamics in inas/gaas quantum dots stimulated by bound-to-continuum excitation," J. Appl. Phys. **113**, 223511 (2013).
18. E. D. Palik, *Handbook of Optical Constants of Solids*, vol. 3 (Academic press, 1998).
19. M. V. C. Synopsys, Inc., "Rsoft Diffractmod User Guide," v2016.09 (2016).

1. Introduction

The Intermediate band solar cell (IBSC) is an attractive concept because of their extremely high efficiency limit of 63% under full concentration [1]. As sketched in Fig. 1, their operating principle is based on the sequential absorption of two sub-bandgap photons - via an IB only optically coupled to the conduction and valence bands - to extend the sun harvesting up to the mid-Infrared (MIR) range, yielding large photocurrent and high voltage [2]. In fact, whereas the photovoltage of single-gap solar cells is limited by the lowest energy of the single photon they can absorb (E_g), in IBSCs a comparable voltage is generated by the absorption of two photons with sub-bandgap energies. [2].

Quantum dots (QDs) are well suited as IB material as they form three-dimensional potential wells that provide bound states fully isolated from the continuum bands owing to their zero-dimensional density of states [2]. Extensive research on III-V QD-IBSCs has allowed the experimental proof of the IBSC operating principles [2, 3]. However, the demonstration of high-efficiency QD-IBSCs remains challenging, *in primis* because of a few fundamental limitations inherent to the QD themselves. As first, the IB operation requires strong absorption coefficients (α_{VI}, α_{IC}) for the sub-bandgap optical transitions [3], but from the practical standpoint their strength is limited by the small optical cross-section of QDs and by the relatively low QD areal density and number of layers that can be used without compromising the solar cell crystal quality. Moreover, thermal and field-activated escape from the bound states forming the IB competes and hinders the second-photon absorption process to such an extent that the observation of two-photon

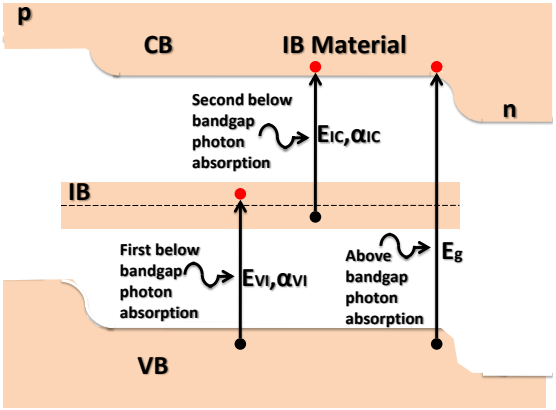

Fig. 1. (a) Schematic band diagram of a IB solar cell highlighting the sub-bandgap optical transistions between valence band and IB (VB→IB) and conduction band and IB (IB→CB), and the above gap (VB→CB) optical transition.

Optics EXPRESS

absorption usually requires cryogenic temperatures. To overcome these limitations, QD material engineering [3] and light trapping approaches are required [4]. Diffraction gratings [5–7] and plasmonics [8] have been investigated to enhance the near infrared (NIR) absorption of QDs and quantum wells. In [9] we have recently reported QD thin-film cells fabricated by epitaxial lift-off demonstrating a two-fold increase of QD NIR photocurrent [9] through the integration of a planar reflector. As for the MIR window, bi-periodic diffraction gratings for QD-IBSCs directly etched in the cell substrate were theoretically studied in [10], pointing out the potential for a large increase of the intraband absorption for QD cells thicker than the sun radiation coherence length.

In this work, we investigate the use of guided-mode resonance (GMR) effects [11] in thin-film QD solar cells to enhance the weak MIR intraband absorption. Resonant waveguide-grating structures patterned on the surface of thin-film silicon cells on quartz substrate were proposed in [12, 13]. Enhancing QD optical transitions in the MIR range is also a key task in the development of QD infrared detectors (QDIP). The use of a GMR grating on the top surface and a distributed Bragg reflector on the bottom has been proposed in [14] to implement resonant-cavity enhanced QDIPs. Taking advantage of the thin-film architecture in [9], we propose here a design wherein the GMR grating is patterned at the rear surface of the cell, leaving room for the optimization of the cell antireflection characteristics through multilayer and/or nanostuctured gratings [15, 16] realized on the top surface of the cell.

2. Theory and design

The GMR operating principle and designed solar structure are sketched in Fig. 2. To exploit waveguide-grating resonances, the solar cell is designed enough thin ($\leq 1\ \mu$m) and integrated with a rear side sub-wavelength grating. As shown in Fig. 2(a), GMR arises when the diffracted orders excited by the grating couple the incoming light into the waveguide modes. Thus, a phase matching condition must occur between the evanescent diffracted waves excited by the grating and the waveguides modes supported by the waveguiding structure [11, 13]. Under the hypothesis

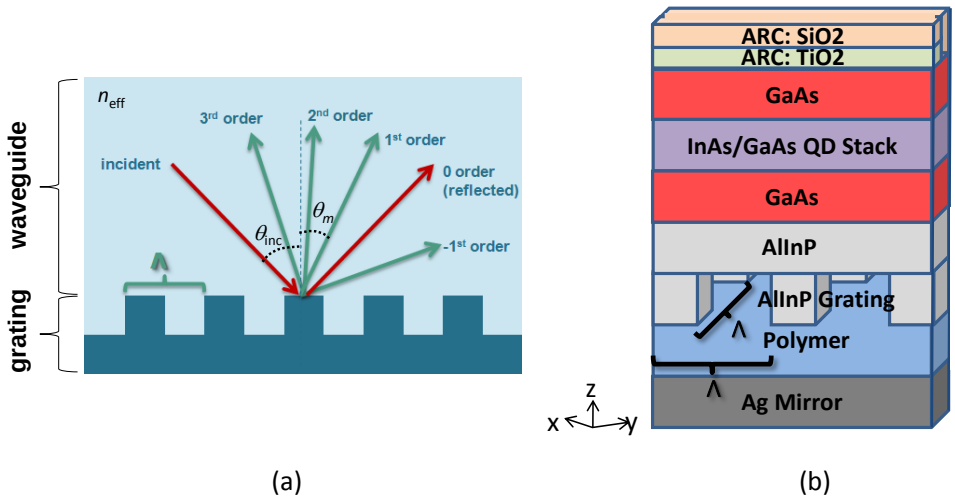

Fig. 2. (a) Schematic sketch of an elementary GMR structure composed of a slab waveguide characterized by effective index n_{eff} with a grating integrated at the rear side. (b) Designed solar cell structure terminated by a three-dimensional cubic grating with period=Λ. The layer thicknesses are: 110 nm - SiO_2, 55 nm - TiO_2, 300 nm - GaAs, 150 nm - QD, 200 nm - GaAs, 82 nm - AlInP, $h = 1200$ nm for the AlInP grating height (varied during optimization), 250 nm - polymer ($n = 1.55$).

Optics EXPRESS

of a 1D grating with weak index modulation, the resonances with a guided mode of effective index n_{eff} may be identified according to the grating equation

$$n_{\text{eff}} = n_{\text{air}} \sin\theta_{\text{inc}} - \frac{m\lambda}{\Lambda} \tag{1}$$

Λ being the grating period, m the diffraction order, λ the incident wavelength, and n_{air} the air refractive index. At normal incidence and cutoff of the grating mode, the resonance condition reads as $n_{\text{eff}} = m\lambda/\Lambda$.

The active region of the cell (Fig. 2(b)) is made of a stack of InAs/GaAs QD layers with overall thickness of 150 nm (10 QD layers with GaAs interdot layers of 10 nm), embedded within two GaAs layers of 300 nm and 200 nm, respectively. The grating is patterned onto the AlInP back surface field layer and terminated by a conformal planarizing polymer layer and a planar Ag mirror to achieve the highest possible reflectivity while preventing parasitic electrical losses and optical loss in the mirror. A conventional two-layer anti-reflection coating (ARC) composed of SiO_2 and TiO_2 is used. In this initial example, the primary VB - IB transition is set to 1.13 eV, and the IB - CB (second low energy photon) transition to 270 meV. The QD stack is modeled as a homogeneous medium with average complex refractive index in the NIR range as calculated in [6]. For the intraband absorption coefficient (α_{IC}) we assume an average constant value of 200 cm^{-1} at $\lambda_{\text{IC}} = 4.6\,\mu\text{m} \pm 0.3\,\mu\text{m}$ in line with experimental data of similar QDs [17], while the real part of the refractive index is assumed equal to the GaAs one. Even though this is not strictly correct, the associated error is expected to be marginal. The optical models of the other materials are taken either from the literature [18] or from experimental characterization [15].

Eqs. 1 provides a simple tool to gain a preliminary understanding of the impact of parameters such as the grating period, material properties, waveguide layers thickness, and angle of incidence on the GMR onset. Fig. 3 shows a few examples of resonance conditions predicted according to eq. 1 for the waveguiding cell structure in Fig. 2(b) and different grating periods, at normal incidence. It is seen that multiple resonances could be sought for in the λ_{IC} range by using grating

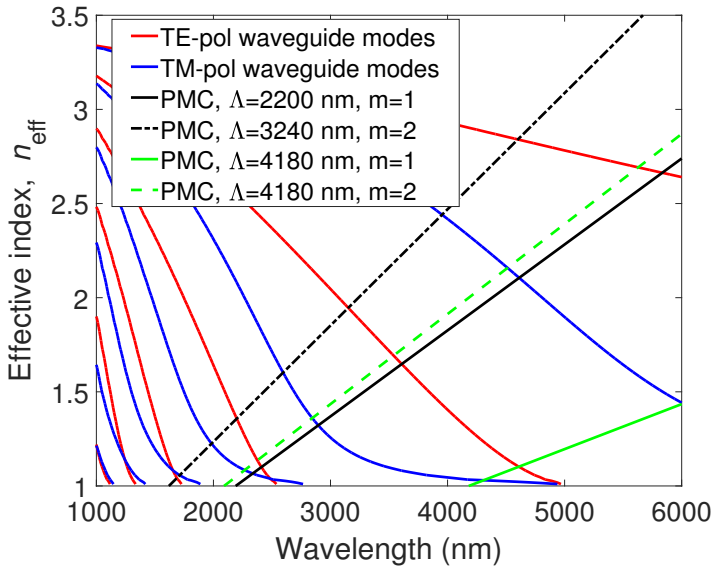

Fig. 3. Effective refractive index of the guided modes *vs.* wavelength, with phase matching conditions for first (m=1) and second (m=2) order modes of linear grating with different periods.

Optics EXPRESS

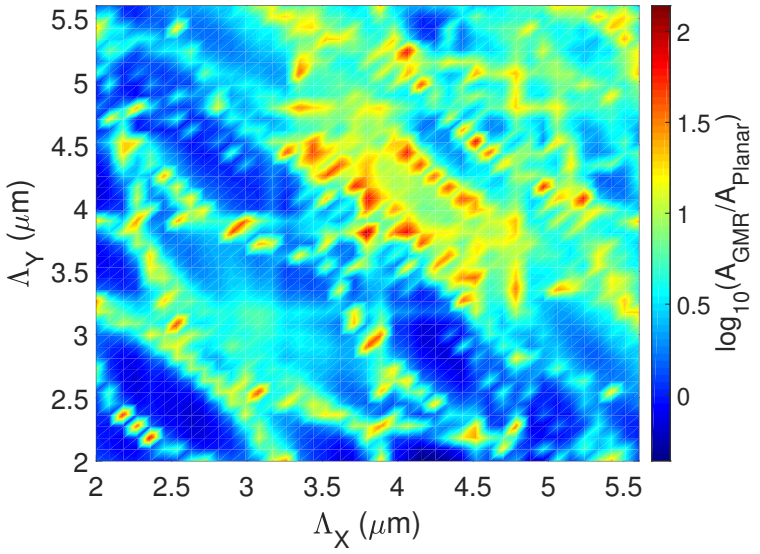

Fig. 4. Map of the peak absorbance enhancement for cubic grating as a function of grating periods in x and y directions.

periods approximately around $3 - 4\,\mu$m.

The GMR effect is achievable with uni-periodic or bi-periodic grating structures implemented using different geometrical shapes including cubic, pyramidal, or half-spherical gratings. In this study, bi-periodic cubic grating structures were simulated with the rigorous coupled-wave analysis (RCWA) method using a commercial software [19]. TE and TM polarizations were assigned equal weight in the simulations. Optimization – aimed at maximizing the absorbance in the QD photoactive region at λ_{IC} for normal incidence – was carried out in terms of period and aspect ratio, with a fixed duty cycle of 0.5. The light-trapping effect is quantified by comparing the absorbance in the QD stack at the center wavelength λ_{IC} (A_{GMR}) for the GMR solar cell with the one of an unpatterned solar cell with identical cross-section (A_{planar}) terminated by the Ag mirror. A preliminary optimization carried out in terms of period and aspect ratio (AR =height/period) pointed out a weak dependence of the GMR effect on the grating height in the AR range $0.2 - 0.6$ and an optimum AR value of about 0.32, in line with previous studies [6]. As shown in Fig. 4, the absorbance enhancement was also studied considering different periods along the x and y directions to verify the influence of different coupling efficiency to the waveguide polarization modes. As expected, the grating is polarization insensitive for direct incidence, and the maximum enhancement ($\Gamma = A_{GMR}/A_{planar} \approx 140$) is found for a symmetric grating with $\Lambda_X = \Lambda_Y = 3.8\,\mu$m. Two secondary maxima ($\Gamma \approx 90$) are found at $\Lambda_X = \Lambda_Y = 2.27\,\mu$m and $\Lambda_X = \Lambda_Y = 4.52\,\mu$m. According to the analytical calculation reported in Fig. 3, it might be argued that the $3.8\,\mu$m period induces phase matching with the fundamental mode and possibly further resonances with higher waveguide modes.

3. Results and discussion

The electric field amplitude and absorbed photon density for the GMR cell and the reference unpatterned cell are shown in Fig. 5, for the optimum grating with period $\Lambda = 3.8\,\mu$m and height $h = 1.2\,\mu$m demonstrating significantly higher electric field and enhanced absorption in the QD stack layer.

Optics EXPRESS

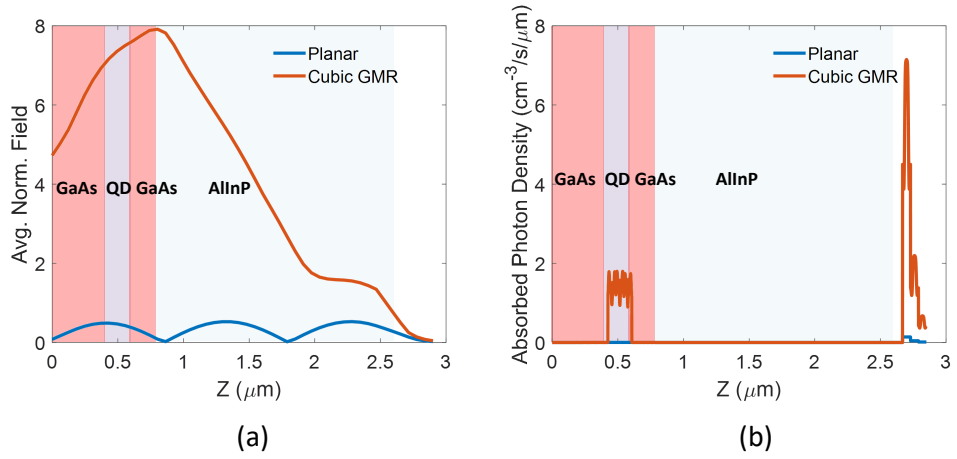

Fig. 5. (a) Average electric field amplitude and (b) average spatial absorbed photon density at $\lambda_{IC} = 4.6\,\mu$m. The spatial profiles are obtained by averaging across the $x - y$ plane.

Fig. 6(a) compares the spectral absorbance ($A(\lambda)$) in the MIR range for the cubic GMR grating and reference planar solar cells. The GMR cell shows a remarkable increase (≈ 156) of $A(\lambda_{IC})$ with respect to the planar one. Based on a simple Lambert-Beer model of the QD stack, at the peak wavelength λ_{IC}, the effective absorption length of the 150 nm thick QD stack is enhanced by a factor larger than 350. Thus, the QD α_{IC} of 200 cm^{-1} turns into an effective absorption of 7×10^4 cm^{-1}, allowing for the absorption of about 65% of the incident photons. In the 60 nm and 600 nm bands around λ_{IC} the absorbance enhancement is ≈ 37 and 15, respectively, resulting into an effective α_{IC} of about 10^4 and 4×10^3 cm^{-1}. It is worth noticing that without exploiting light-trapping such high values of the effective α_{IC} could be reached only with QD stack embedding very high in-plane density and/or number of QD layers, well above values achievable with state-of-art QD growth technologies. Finally, Fig. 6(b) shows that also in the visible-NIR range the GMR cells demonstrates improved light trapping at wavelengths beyond the GaAs bandgap ($\lambda = 0.895 - 1.2\,\mu$m), leading to QD photocurrent increase from ≈ 0.5 mA/cm^2 in the planar mirrored cell to ≈ 1 mA/cm^2 in the GMR cell.

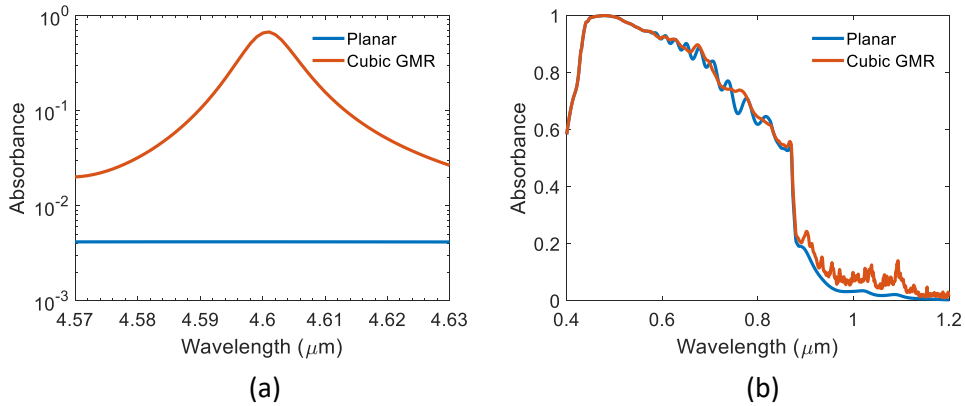

Fig. 6. Absorbance spectra of the optimum GMR structure and the planar structure in the (a) MIR - QD intraband optical transition - and (b) visible-NIR - GaAs and QD interband transitions - ranges.

Optics EXPRESS

The angular selectivity of the maximum absorbance enhancement is analyzed in Fig. 7. For the sake of comparison, we report also the behavior of a half-spherical GMR grating with radius of $\Lambda/4$ and period ($\Lambda = 5.6\mu$m) optimized to attain the highest possible average absorbance enhancement over the $0^o - 90^o$ range. As expected, light-trapping enhancement above the Lambertian limit implies significant angular selectivity. However, for angles of incidence (θ) up to 9^o, corresponding to a concentration factor slightly higher than 1000 sun ($46000 \times \sin^2(\theta)$), the absorbance enhancement is still high (48) and close to the Lambertian limit. The results compare favorably with the previous studies on the GMR effects in silicon solar cells and QDIPs. In [12] three-fold absorbance enhancement was predicted over a 120 nm bandwidth next to the silicon gap and $\pm 40^o$ angle of incidence, while a 30% integrated absorbance enhancement in the 450 nm -750 nm range was experimentally demonstrated for amorphous silicon cells in [13]. Finally, the resonant-cavity enhanced QDIP in [14] showed absorbance enhancement of 20 at the target wavelength of 8 μm for $\pm 10^o$ angle of incidence.

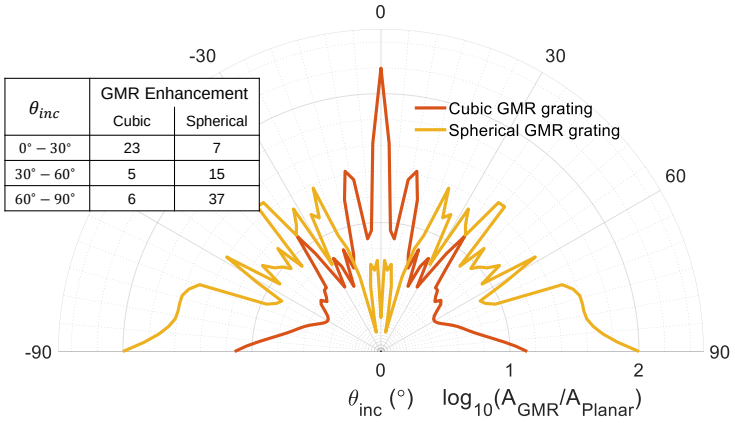

θ_{inc}	GMR Enhancement	
	Cubic	Spherical
$0^\circ - 30^\circ$	23	7
$30^\circ - 60^\circ$	5	15
$60^\circ - 90^\circ$	6	37

Fig. 7. GMR Gain vs. angle of incidence θ_{inc} for the cubic ($\Lambda = 3.8\ \mu$m) and the half-spherical grating ($\Lambda = 5.6\ \mu$m) at wavelength $\lambda_{\text{IC}} = 4.6\ \mu$m.

The IB energy and optical properties depend on several QD parameters such as size and materials. Moreover, α_{IC} is difficult to know. Finally, it can also be reminded that the full optimization of the IBSC operation implies a strict relation between interband and intraband absorption coefficients and the E_{IC} transition energy [3]. Therefore, it is worth to briefly discuss about the scaling of the optimum grating parameters and of the attainable absorbance enhancement with respect to the intraband absorption strength and energy. Fig. 8(a) reports the GMR enhancement at the peak wavelength as a function of the QD intraband optical coefficient showing significant absorbance enhancement (≈ 50) up to $\alpha_{\text{IC}} = 1000\ \text{cm}^{-1}$. In Fig. 8(b), we analyze how the optimum grating period and aspect ration scale as E_{IC} varies from 270 meV to 600 meV, a range representative of the MIR range wavelengths covered by intraband and intersubband transitions in type-I InAs/GaAs and type-II GaAs/GaSb QDs. A weak sensitivity to the aspect ratio is also observed. As anticipated from the analytical model in Fig. 2 decreasing the grating period causes a blue-shift of the resonance wavelengths. In line with this, RCWA simulation results show a decreasing nearly linear trend of the optimum period with E_{IC}. Deviations from a perfect linear behavior are caused by slight changes also of the absorbance of the planar reference. With the optimized period, the GMR enhancement is always found larger than 100 except for the point at highest energy (E_{IC}) where it is limited to about 55, owing to the relatively higher absorbance found in the planar structure. Finally, from the approximated linear dependence of Λ *vs.* E_{IC} we can estimate the sensitivity of the proposed design to fabrication tolerances. From

Optics EXPRESS

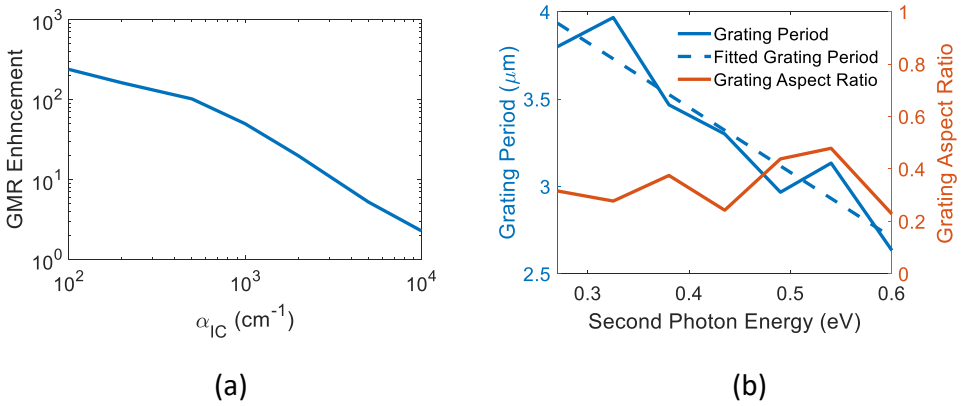

Fig. 8. (a) GMR enhancement *vs.* QD intraband optical absorption coefficient (α_{IC}) at the peak wavelength. (b) Estimated optimum grating period and aspect ratio (height/period) as a function of the second photon absorption energy (E_{IC}). All the optimum points except the one at highest energy (see text) identify GMR enhancement larger than 100 at E_{IC}.

the extracted slope $\Delta\Lambda/\Delta E_{IC} \approx -3.7$, a maximum shift of ± 300 nm of the peak absorbance wavelength with respect to the target one ($\lambda_{IC} = 4.6\mu$m) requires a maximum variation of the period of about ±65 nm, compatible with grating fabrication tolerances.

4. Conclusion

Overcoming the efficiency limitation of single-gap solar cells motivates investigating IB solar cells, which promise high current and high voltage through the absorption of two sub-bandgap photons. We have shown that optical path elongation and resonant field enhancement for lower energy photons are made possible using GMR gratings. The GMR gratings are employed primarily for enhancement of the second photon absorption in the MIR-range for direct and oblique incidence angles. Design guidelines are presented for ranges of energy and strength of the second-photon absorption representative of III-V QDs such as InAs/GaAs and GaSb/GaAs systems. The results demonstrate that the GMR concept is suitable for a wide class of QD-IBSCs. An added benefit of the proposed GMR design is the diffraction at NIR wavelengths which strengthen the primary photon absorption too. These effects will result in improved short circuit current density and IB photogeneration rate. Finally, the structure and approach investigated in this work may also find important application in intraband quantum-dot infrared detectors.

Funding

European Union's Horizon 2020 (H2020) Grant Agreement 687253; COST Action MP1406 (COST-STSM-MP1406-36331).

Acknowledgments

Portions of this work were presented at the Light, Energy and the Environment Congress in 2017, paper PM3A.4. The authors wish to acknowledge Prof. Mircea Guina and Timo Aho, with the Laboratory of Photonics at Tampere University of Technology, for useful discussions.